Published in final edited form as:
Biomaterials. 2012 September ; 33(26): 6186–6193. doi:10.1016/j.biomaterials.2012.05.029.

Theranostic nanoparticles based on PEGylated hyaluronic acid for the diagnosis, therapy and monitoring of colon cancer

Ki Young Choi[a,b,1], **Eun Jung Jeon**[c,1], **Hong Yeol Yoon**[a,d], **Beom Suk Lee**[a,e], **Jin Hee Na**[a,f], **Kyung Hyun Min**[a,f], **Sang Yoon Kim**[e], **Seung-Jae Myung**[g], **Seulki Lee**[b], **Xiaoyuan Chen**[b], **Ick Chan Kwon**[a], **Kuiwon Choi**[a], **Seo Young Jeong**[f], **Kwangmeyung Kim**[a,**], and **Jae Hyung Park**[d,*]

[a]Biomedical Research Center, Korea Institute of Science and Technology, Seoul 136-791, Korea

[b]Laboratory of Molecular Imaging and Nanomedicine (LOMIN), National Institute of Biomedical Imaging and Bioengineering (NIBIB), National Institutes of Health (NIH), Bethesda, MD 20892

[c]Department of Internal Medicine, The Catholic University of Korea School of Medicine, Seoul, Korea

[d]Department of Polymer Science and Engineering, Sungkyunkwan University, Suwon 440-746, Republic of Korea

[e]Department of Otolaryngology, Asan Medical Center, University of Ulsan College of Medicine, Seoul 138- 736, Korea

[f]Department of Life and Nanopharmaceutical Sciences, Kyung Hee University, Seoul 130-701, Korea

[g]Department of Internal Medicine and Asan Digestive Disease Research Institute, Asan Medical Center, University of Ulsan College of Medicine, Seoul 138-736, Korea

Abstract

Colon cancer is the second leading cause of cancer-related death in the United States. The considerable mortality from colon cancer is due to metastasis to other organs, mainly the liver. In the management of colon cancer, early detection and targeted therapy are crucial. In this study, we aimed to establish a versatile theranostic system for early tumor detection and targeted tumor therapy by using poly(ethylene glycol)-conjugated hyaluronic acid nanoparticles (P-HA-NPs) which can selectively accumulate in tumor tissue. For the diagnostic application, a near-infrared fluorescence (NIRF) imaging dye (Cy 5.5) was chemically conjugated onto the HA backbone of P-HA-NPs. After intravenous injection of Cy5.5-P-HA-NPs into the tumor-bearing mice, small-sized colon tumors as well as liver-implanted colon tumors were effectively visualized using the NIRF imaging technique. For targeted therapy, we physically encapsulated the anticancer drug, irinotecan (IRT), into the hydrophobic cores of P-HA-NPs. Owing to their notable tumor targeting capability, IRT-P-HA-NPs exhibited an excellent antitumor activity while showing a reduction in undesirable systemic toxicity. Importantly, we demonstrated the theranostic application using Cy5.5-P-HA-NPs and IRT-P-HA-NPs in orthotopic colon cancer models. Following the systemic administration of Cy5.5-P-HA-NPs, neoplasia was clearly visualized, and the tumor growth was effectively suppressed by intravenous injection of IRT-P-HA-NPs. It should be emphasized that the therapeutic responses could be simultaneously monitored by Cy5.5-P-HA-NPs. Our results

[*]Corresponding author: Theranostic Macromolecules Research Center Department of Polymer Science and Engineering Sungkyunkwan University, Suwon 440-746, Republic of Korea Tel: +82-31-299-6859; fax: +82-31-292-8790; jhpark1@skku.edu.
[**]Co-corresponding author: Biomedical Research Institute Korea Institute of Science and Technology, Seoul 136-791, Korea Tel: +82-2-958-5916; fax: +82-2-958-5909; kim@kist.re.kr.
[1]These authors contributed equally

suggest that P-HA-NPs can be used as a versatile theranostic system for the early detection, targeted therapy, and therapeutic monitoring of colon cancer.

Keywords

Hyaluronic acid; nanoparticle; theranostics; irinotecan; colon cancer; tumor targeting

1. Introduction

Colon cancer causes approximately 50,000 deaths in the United States and 655,000 deaths throughout the world per year [1, 2]. As of 2010, colon cancer was the second leading cause of cancer-related death in the United States [1]. Given the considerable mortality from colon cancer due to metastasis to other organs, early detection is highly essential for management of colon cancer. If detected at an early stage, colon cancer can be prevented by the removal of adenomatous polyps [3-5]. However, in many cases, colon cancer is detected in late stages due to the poor sensitivity and specificity of conventional screening methods. Although a variety of screening modalities, including fecal occult blood test [6], sigmoidoscopy [7], optical colonoscopy [8] and virtual colonography [9], have been developed, the miss rate of colon cancer is still considerable. For instance, the overall miss rate of colonoscopy is 24%. Furthermore, the miss rate increases up to 27% for flat and depressed neoplasms or adenomas smaller than 5 mm [10, 11].

The failure of colon cancer detection allows for metastases to other organs. It has been reported that almost 70% of colon cancer patients are diagnosed with metastatic disease. Of the patients with metastatic colon cancer, more than 70% experience hepatic metastases [12]. Nevertheless, treatments of patients with metastatic colon cancer are highly limited because a considerable proportion of metastatic colon cancer is unresectable. For the treatment of metastatic colon cancer, chemotherapeutics with various combinational regimens have been widely considered a viable treatment option [13-16]; however, systemic chemotherapy has an insufficient therapeutic efficacy. In addition, undesirable biodistribution of anti-cancer drugs following systemic administration causes severe side effects. Furthermore, the systemic toxicity limits the injectable drug doses and thereby further lowers the therapeutic efficacy. To overcome these drawbacks in current diagnostic and therapeutic systems, it is necessary to develop a novel system that enables early diagnosis and targeted therapy [17].

Our group has developed poly(ethylene glycol) (PEG)-conjugated hyaluronic acid nanoparticles (P-HA-NPs) for tumor targeting [18, 19]. In previous studies, we demonstrated that systemic administration of P-HA-NPs resulted in selective accumulation of the nanoparticles in tumor tissue through the enhanced permeation and retention effect [20-23] and strong receptor binding to the HA receptor (CD44), which is over-expressed in various cancer cells [24-29]. In addition, P-HA-NPs hold great potential for tumor theranostics, owing to their physicochemical flexibility. Due to plentiful functional groups including carboxylic acid and hydroxyl groups on the HA backbone, P-HA-NPs can be modified with various diagnostic agents or therapeutic molecules. Moreover, P-HA-NPs can also accommodate hydrophobic molecules like imaging agents and anticancer drugs in their hydrophobic inner cores via hydrophobic interactions [19]. These tumor-targeting attributes and multifunctionalities of P-HA-NPs offer promising possibilities for the early diagnosis and targeted therapy of colon cancer. Despite the great potential of P-HA-NPs for theranostics, the detailed application has not been yet explored.

Therefore, in this study, we aimed to establish a potent theranostic system based on P-HA-NPs for early diagnosis and targeted therapy of colon cancer. To evaluate the theranostic efficacy of P-HA-NPs, we labeled P-HA-NPs with a near-infrared fluorescent (NIRF) dye, Cy5.5, through chemical conjugation and physically encapsulated the anticancer drug irinotecan (IRT) into the hydrophobic cores of the nanoparticles. The theranostic potential of the P-HA-NPs was assessed in various mice colon cancer models including HT29 human colon cancer xenografts, liver-implanted colon cancer models, and orthotopic colon cancer models.

2. Materials and Methods

2.1. Materials

Sodium hyaluronate (MW = 2.344×10^5 Da, Lifecore Biomedical, Chaska, MN) was used after dialysis against distilled water, followed by lyophilization. 5β-cholanic acid (CA), monomethoxy PEG-amine (mPEG, MW = 5 kDa), 1-ethyl-3(3-dimethylaminopropyl) carbodiimide (EDC), adipic acid dihydrazide (ADH), 1-hydroxybenzotriazole (HOBt), irinotecan hydrochloride (IRT), and azoxymethane (AOM) were obtained from Sigma-Aldrich Co. (St. Louis, MO, USA). Dextan sodium sulfate (DSS) was purchased from MP Biochemicals, LLC (Aurora, OH, USA). The NIR dye (Cy5.5) was purchased from Amersham Biosciences (Piscataway, NJ, USA). The water used for synthesis and characterization was purified via distillation, deionization, and reverse osmosis (Milli-Q Plus). HT29 (colon cancer cells) and CT26 (colon cancer cells) were purchased from the American Type Culture Collection (Rockville, MD, USA). All other chemicals were analytical grade and used without further purification.

2.2. Preparation and characterization of theranostic P-HA-NPs

2.2.1. Cy5.5-labeled P-HA-NPs—The synthetic details are described in our previous reports.[18, 19] To synthesize amphiphilic HA-5β-cholanic acid conjugate bearing ten 5β-cholanic acids per 100 sugar residues of HA, the hydrophilic HA polymer was chemically modified with a hydrophobic bile acid CA through amide formation. Furthermore, mPEG-HA-CA conjugates, modified with five mPEG per 100 sugar residues of HA, were prepared via chemical conjugation of mPEG-amine into the HA backbones on the surface HA-NPs in the presence of EDC and HOBt. The resulting conjugates were purified through dialysis. The PEG content in the conjugate was determined using ^{1}H NMR (600MHz Superconducting FT-NMR Spectrometer, Varian, CA, USA), for which the sample was prepared by dissolving the conjugate in D_2O/CD_3OD (1v/1v). The particle sizes of the HA-NPs were measured at the concentration of 1 mg/ml using a dynamic light scattering (DLS) system. For the diagnostic applications of P-HA-NPs, the conjugates were labeled with the near infrared fluorophore, Cy 5.5.

2.2.2. IRT-loaded P-HA-NPs—To evaluate the anti-cancer efficacy of P-HA-NPs, we prepared IRT-loaded P-HA-NPs (IRT-P-HA-NPs) using the O/W emulsion method. In detail, 20 mg of P-HA-NPs were dispersed in 20 ml of DW. IRT was dissolved in cold DW, and 1.5 molar equivalents of hydrochloric acid was added to the IRT solution with stirring. After precipitation, the IRT solution was filtered through a 0.45-μm filter membrane, and then precipitates remaining on the filter membrane were washed twice with cold water prior to freeze-drying. The resulting powder was dissolved in methylene chloride at predetermined concentrations. The IRT solutions were added into the P-HA-NP solutions drop-wise with sonication, followed by dialysis against distilled water to remove unloaded drugs and organic solvent, and then lyophilized. When the resulting samples were dispersed in phosphate-buffered saline (PBS, pH 7.4) by sonicating three times for 2 min each using a probe-type sonifier (VCX-750, Sonics & Materials, CT, USA) at 90 W, the nanoparticles

readily formed. The sizes of the IRT-P-HA-NPs were measured using dynamic light scattering (DLS). The concentration of nanoparticles was kept constant at 1 mg/ml. The loading content of IRT in P-HA-NPs was determined using a UV spectrometer at 365 nm.

2.3. Diagnostic application of Cy5.5-P-HA-NPs using an NIRF imaging technique

In vivo real-time NIRF imaging was achieved using the eXplore Optix system (ART Advanced Research Technologies Inc., Montreal, Canada). All of the data were calculated using the region of interest (ROI) function of the Analysis Workstation software (ART Advanced Research Technologies Inc., Montreal, Canada), and values are presented as means ± SE for groups of three animals. The fluorescence images of the Cy5.5-P-HA-NPs in dissected organs and tumors were obtained using a Kodak imaging box in the same manner as previously reported.[18, 19]

2.3.1. HT29 human colon cancer xenograft—HT29 human colon cancer xenografts were prepared as follows. Three male BALB/c nude mice (seven weeks old, 20-25 g) were acclimatized to tap water and an ad libitum basal diet for seven days. A suspension of 1×10^7 HT 29 cells in physiological saline (100 μl) was injected into the subcutaneous dorsa of the nude mice. These mice were maintained on a basal diet and tap water. When the tumor diameter reached around 5 mm, Cy5.5-P-HA-NPs were injected into the tail vein of the HT29 human colon cancer xenografts to evaluate the diagnostic efficacy. *In vivo* whole body images of Cy5.5-P-HA-NPs in live animals were obtained at predetermined time points. At 48 h after injection, mouse organs and tumors were removed, and fluorescence signals for Cy5.5-P-HA-NPs were detected in the dissected organs and tumors using a Kodak imaging box.

Intravital tumor tissue images were obtained using an Olympus OV100 and IV100 Intravital Scanning Laser Microscope (Olympus Corp., Tokyo, Japan). To visualize tumor tissue, the HT29 colon cancer xenografted mice were anesthetized with 2 % isoflurane in 2 l/min O_2. The tumor tissue was then exposed by creation of an incision in the skin at the tumor site, followed by intravenous injection of fluorescein isothiocyanate (FITC)-labeled dextran (10 mg/kg) to visualize the tumor vasculature and injection of Cy5.5-P-HA-NPs (5 mg/kg) to monitor their traces in the tumor tissue. At 1 h after i.v. injection of both molecules, NIRF intravital tumor tissue images were obtained.

2.3.2. AOM-induced orthotopic colon cancer model—Azoxymethane (AOM) treatment in A/J mice has been shown to induce colon tumors that mimic the adenoma-to-carcinoma sequence of sporadic colon cancer in humans.[30] Four male A/J mice (Japan SLC, Inc., Hamamatsu, Japan) aged five weeks were acclimatized to tap water and an ad libitum basal diet for seven days. Three mice were injected intraperitoneally with 10 mg/kg body weight of AOM (Sigma-Aldrich Co. St. Louis, MO) in saline once per week for six weeks. These mice, as well as an untreated control mouse, were maintained on a basal diet and tap water. In a previous study,[31] it was demonstrated that tumors were induced in the colons of mice treated with AOM at 12 weeks after the final injection of AOM, and the number of tumors increased with time. At 20 weeks after the final injection, the number of tumors as well as the ratio of adenocarcinomas to adenomas significantly increased. Accordingly, Cy5.5-P-HA-NPs were injected into the tail veins of AOM-induced colon cancer models to evaluate the diagnostic efficacy of Cy5.5-P-HA-NPs at 20 weeks after the final injection of AOM. Six hours later, three orthotopic colon cancer mice and one control mouse were sacrificed, and the colons were surgically excised and examined using the eXplore Optix system and a Kodak imaging box.

2.3.3. Liver-implanted colon cancer model—A liver-implanted colon cancer model was established by inoculating the left lobe of the liver with murine colon cancer cells (CT26), as described in a previous report.[32] Three male BALB/c nude mice (seven weeks old, 20-25 g) were acclimatized to tap water and an ad libitum basal diet for seven days. Two mice were anesthetized with intraperitoneal (i.p.) injections of ketamine and xylazine. After anesthesia, laparotomy was performed with direct injection of 3×10^5 CT26 mice colon cancer cells in 20 μl of saline into the left lobe of the liver. These mice were maintained on a basal diet and tap water. At 14 days after subcutaneous inoculation with CT26 colon cancer cells, Cy5.5-P-HA-NPs were injected into the tail vein of the liver-implanted colon cancer models to evaluate the diagnostic efficacy. *In vivo* whole body images of Cy5.5-P-HA-NPs in live animals were obtained at predetermined time points. At 48h after injection, mouse organs were removed, and fluorescence images for Cy5.5-P-HA-NPs in dissected organs and tumors were acquired using a Kodak imaging box.

2.4. Therapeutic application of IRT-P-HA-NPs for colon cancer treatment

To evaluate the antitumor efficacy of IRT-P-HA-NPs, HT29 tumor-bearing mice were prepared as described above. Mice were divided into three groups: (i) normal saline (the control group), (ii) free IRT at 10 mg/kg, and (iii) IRT-P-HA-NPs at 10 mg IRT/kg. Once tumors reached 5 mm in diameter, each sample was injected once every three days, for a total of five injections. The survival rates of the mice were recorded, and tumor volumes were calculated as $a \times b^2 \times 0.52$, with a and b being the largest and smallest diameters, respectively. Histological changes in major organs and tumor tissues were evaluated using hematoxylin and eosin (H&E) staining methods.

2.5. Therapeutic monitoring of IRT-P-HA-NPs using Cy5.5-P-HA-NPs

Twenty-four male BALB/c mice were acclimatized to tap water and an ad libitum basal diet for seven days. Twenty-one mice received a single intraperitoneal injection of AOM (10 mg/kg body weight) and, commencing one week later, these animals were given drinking water containing 2% (w/v) DSS for seven days, followed by maintenance on a basal diet and tap water. The remaining three mice received the basal diet and tap water throughout the experiment. In a previous report [31], we demonstrated that tumors were induced in the colons of mice treated with AOM/DSS at six weeks after the final administration of DSS, and the number of tumors increased with time. In this study, to detect tumorigenesis of Cy5.5-P-HA-NPs, we intravenously injected Cy5.5-P-HA-NPs into the three AOM/DSS-induced orthotopic colon cancer models at 12 weeks after the final administration of DSS. Six hours later, the mice were sacrificed, and the colons were surgically excised and examined using the eXplore Optix system. After monitoring neoplasia in the mice models, we divided the remaining 18 mice into three groups: (i) normal saline (the control group), (ii) free IRT at 10 mg/kg, and (iii) IRT-P-HA-NPs at 10 mg IRT/kg. Each sample was injected once every three days, for a total of five injections. At 40 days after the start of therapy, we intravenously injected Cy5.5-P-HA-NPs into the 18 AOM/DSS-induced mice and three control mice to monitor therapeutic responses to the administration of IRT-P-HA-NPs. Six hours later, mice were sacrificed, and the colons were surgically excised and examined using the eXplore Optix system. For polyp examination, colons were retrieved and fixed in 4% (v/v) buffered formalin solution, dehydrated with a graded ethanol series, and embedded in paraffin. The paraffin tissue was sliced to obtain 6-μ-thick sections. Paraffin-embedded colon sections were stained using H&E staining methods. Polyps were examined under a dissection microscope by an experienced pathologist at the Catholic Medical Center as previously reported [33].

2.6. Statistical analysis

The statistical significances of differences between groups were determined using a one-way ANOVA. A $p<0.05$ was considered significant and is specified in the figures with an asterisk.

3. Results and Discussion

3.1. Preparation and characterization of theranostic P-HA-NPs

In an effort to develop a tumor-targeted theranostic system, we prepared self-assembled P-HA-NPs containing either an antitumor drug IRT or a NIRF dye Cy5.5. First, we prepared amphiphilic PEG-HA-5β-cholanic acid conjugates, as previously described [18, 19]. Owing to their amphiphilic properties, the resulting conjugates were self-associated in an aqueous condition, readily forming P-HA-NPs (256 nm in diameter), as listed in Table 1. Second, the P-HA-NPs were chemically labeled with Cy5.5 on their HA shell for diagnostic application. Moreover, the hydrophobic anticancer drug IRT was physically loaded into the hydrophobic inner cores of the nanoparticles using an O/W emulsion method. Interestingly, the particle sizes of P-HA-NPs decreased once the IRT was loaded. This phenomenon may be due to the fact that the drug-loading process results in a more compact nanostructure of P-HA-NPs through hydrophobic interactions between IRT and the hydrophobic inner cores of P-HA-NPs. The particle sizes of the IRT-P-HA-NPs increased with the feed ratio. As the feed ratio increased by over 40%, the particle size sharply increased, resulting in a diameter of 404 nm. On the other hand, the loading efficiency of the IRT gradually decreased as the feed ratio of the IRT increased. When the feed ratio increased by over 30%, the loading content did not significantly increase, although the feed ratio increased. Therefore, IRT 30%-P-HA-NPs, which had an approximate diameter of 238 nm and a loading content of 19%, were chosen for use in further experiments. The *in vitro* drug release rate and cytotoxicity tests of IRT-P-HA-NPs were also carried out. IRT was gradually released from nanoparticles within 12 hours (Supporting Information Figure S2) and exerted a dose-dependent cytotoxicity to HT29 human colon cancer cells (Supporting Information Figure S3). The nanoparticles exhibited cytotoxicity comparable to free IRT at low concentrations (0.5, 5 and 50 μg/ml) and slightly superior at a high concentration (100 μg/ml). Because HT29 cells are known to over-express CD44 [34, 35], the increase in cytotoxicity can be explained by the efficient, receptor-mediated endocytosis of IRT-P-HA-NPs loaded with IRT.

3.2. Diagnostic application of Cy5.5-P-HA-NPs

We employed Cy5.5-P-HA-NPs to evaluate their diagnostic potential for the critical early detection of tumors in both HT29 human colon cancer xenografts and azoxymethane (AOM)- induced orthotopic colon cancer models.

3.2.1. Diagnosis of small-sized HT 29 colon tumors—First, we tested the efficacy of Cy5.5-P-HA-NPs for detecting small tumors—approximately 5 mm in diameter—in HT29 human colon cancer xenografts. As shown in Figure 1a, the tumors inoculated on the dorsa of the nude mice were clearly visualized 1 h after Cy5.5- P-HA-NP injection. Interestingly, Cy5.5-P-HA-NPs were rapidly extravasated from the blood vessel into the tumor tissue and were evenly distributed in the tumor tissue at 1 h (Fig. 1b). The fluorescence signals in tumors continued to increase up to 6 h post injection and then gradually decreased with time. Whole body imaging, on the other hand, exhibited only weak signals and rapidly decreased 1 h post injection. The average fluorescence signals for tumors increased nearly three-fold compared to the whole body signals at 48 h post injection (Fig. 1c). With time, tumor tissues were clearly distinguished from normal tissues. The excellent diagnostic potential of P-HA-NPs was also confirmed with *ex vivo* NIRF images (Fig. 1d). Furthermore, CD44 expression in HT29 tumor tissues was evaluated by histological analysis. As shown in

Supporting Information Figure S4a, a great expression of CD44 was observed in HT29 tumor tissues.

3.2.2. Diagnosis of early-stage orthotopic colon tumors—Early-stage tumors in an orthotopic colon cancer model were also monitored using Cy5.5-P-HA-NPs. For clinical applications, it is of high importance to confirm the diagnostic potential of Cy5.5-P-HA-NPs in a human-like colon cancer model. The AOM-induced orthotopic colon cancer model closely resembles human sporadic colon cancer because it shows the adenoma-to-carcinoma sequence characteristic of human colon cancer. As shown in Figure 2a, NIRF signals clearly delineated the margin of adenomas as well as carcinomas after the systemic administration of Cy5.5-P-HA-NPs. It is important to note that, although the polyps were very small (approximately 1~3 mm in diameter) and at an early stage (adenoma stage), their strong fluorescence intensities were markedly distinguished from the background signals, resulting in excellent colon cancer detection.

3.2.3. Diagnosis of liver-implanted orthotopic colon tumors—Hepatic metastases of colon cancer contribute to the considerable death rate of patients. To decrease mortality by colon cancer, the metastases should be monitored in parallel with treatment. In this study, a liver-implanted CT26 colon cancer model was prepared to mimic liver-metastatic colon cancer, and the diagnostic potential of Cy5.5-P-HA-NPs was evaluated after systemic administration. Figure 3a shows *in vivo* real-time NIRF images of liver-implanted colon cancer models. Following intravenous injection of Cy5.5-P-HA-NPs, the colon tumors implanted into the liver tissue were clearly detected *in vivo*. From the *in vivo* images, it was possible to estimate the size and location of tumors. *Ex vivo* organ images clarified that the strong NIRF signals of *in vivo* whole body images precisely corresponded to tumor sites (Fig. 3b). Further analysis of the tumor sites confirmed liver tumorigenesis by tissue analysis (Fig. 3c).

3.3. Therapeutic application of IRT-P-HA-NPs for colon cancer treatment

The therapeutic efficacy of P-HA-NPs loaded with IRT (IRT-P-HA-NPs) was evaluated using the animal model with HT29 colon cancer. The tumor volume and the survival rate of the mice were determined after intravenous injections of IRT-P-HA-NPs at a dose of 10 mg IRT/kg into the tumor-bearing mice once every three days (Figure 4a, b). The saline-treated control group exhibited a rapid increase in tumor size over time. The group treated with free IRT also showed significant tumor growth. In contrast, significant suppression of tumor growth was observed in the group treated with IRT-P-HA-NPs, suggesting that IRT-P-HA-NPs have a high therapeutic efficacy. Figure 4b shows the survival rate of the mice treated with each of the different samples. Surprisingly, 50% of mice treated with free IRT died after 15 days, and nearly 90% of mice had died within 28 days, indicating that IRT has severe systemic toxicity. However, the group treated with IRT-P-HA-NPs exhibited a higher survival rate than either the positive or negative control groups; more than 60% of the mice survived up to 28 days. To scrutinize their therapeutic efficacy and systemic toxicity, we further collected histological images of major organs and tumors using the H&E staining method (Figure 4c and Supporting Information Figure S5). As expected, the images suggested that IRT-P-HA-NPs effectively eradicated the tumor tissue, whereas only piecemeal necrosis was observed in the liver tissues. However, severe diffuse necrosis was found in greater than 70% of liver tissues of the IRT-treated mice. This severe liver toxicity of IRT might account for the poor survival rate of IRT-treated mice. These results demonstrate that conventional treatment with IRT can adversely affect liver tissues, inducing undesirable systemic toxicity. On the other hand, IRT-P-HA-NPs specifically delivered IRT into the tumor tissues and effectively suppressed tumor growth with limited systemic toxicity.

3.4. Therapeutic monitoring of IRT-P-HA-NPs using Cy5.5-P-HA-NPs

Based on the above diagnostic and therapeutic results, the applications of P-HA-NPs were extended to therapeutic monitoring. Since colon cancer is a rapidly progressing disease that easily metastasizes to other organs, therapeutic monitoring and personalized treatment are imperative for effective therapy. Here, we evaluated the theranostic efficacy of P-HA-NPs in AOM/dextan sodium sulfate(DSS)-induced orthotopic colon cancer models according to the predetermined administration plan. First, to determine the effect of Cy5.5-P-HA-NPs on tumorigenesis, we randomly selected three mice for intravenous injections of Cy5.5-P-HA-NPs. The NIRF images revealed considerable tumorigenesis in all colons tested (Figure 5a). The histological results confirmed that polyps, detected in the NIRF images, included an average of approximately three cancerous lesions and five polypoid lesions per colon (Figure 5b). Moreover, the immunohistochemical results exhibited a considerable amount of CD44 expressed in an AOM/DSS-induced colon tumor tissue by comparison with a normal colon tissue (Supporting Information Figures S4b, c). Thereafter, the mice were administered by three kinds of samples: (i) normal saline (the control group), (ii) free IRT at 10 mg/kg (the IRT group), and (iii) IRT-P-HA-NPs at 10 mg IRT/kg into the remaining mice (the IRT-P-HA-NP group). At 40 days, we intravenously injected Cy5.5-P-HA-NPs into the mice to monitor therapeutic responses. As shown in Figure 5a, the therapeutic responses to the IRT-P-HA-NPs were monitored using a simple NIRF imaging technique, and resulted in clear differentiation in the therapeutic efficacies among the groups.

It was not surprising that, among all groups tested, the most significant tumor growth was detected in the control group. The IRT-P-HA-NP group exhibited significant suppression of tumor growth, demonstrating the effective therapeutic efficacy of IRT-P-HA-NPs. The fluorescence intensities of the IRT-P-HA-NP group were notably lower than those of the other groups. The average number of cancerous lesions (4.6 in the IRT-P-HA-NP group vs. 8 in the control group and 6 in the IRT group) and tumor weight (0.29 g in the IRT-P-HA-NP group vs. 1.1 in the control group and 0.52 in the IRT group) were also significantly lower compared to those in the other groups ($P < 0.05$).

The above results demonstrate that P-HA-NPs can be used as a platform nanocarrier for tumor theranostics. The use of P-HA-NPs enables the detection of tumors at an early stage and also significantly suppresses tumor growth, while reducing severe systemic toxicity. Furthermore, therapeutic responses can be monitored with P-HA-NPs, which may facilitate rapid therapeutic decisions.

4. Conclusions

Improved management of colon cancer greatly depends of the development of a versatile theranostic system that enables early detection and targeted therapy to improve current techniques that have a high miss rate of colon cancer leading to metastases. In this study, we created a theranostic carrier system based on PEGylated HA nanoparticles containing either NIRF imaging dye (Cy 5.5) or an anticancer drug (IRT). With intravenously injected Cy5.5-P-HA-NPs, small-sized and early-stage colon tumors as well as liver-implanted colon tumors were effectively visualized using a NIRF imaging technique. Owing to their remarkable tumor targeting ability, IRT-P-HA-NPs exhibited significant suppression of tumor growth with a reduced systemic toxicity. Furthermore, the therapeutic responses could be simultaneously monitored with Cy5.5-P-HA-NPs. Our results suggest that the P-HA-NPs have promising potential as theranostic nanoparticles for effective tumor therapy.

Supplementary Material

Refer to Web version on PubMed Central for supplementary material.

Acknowledgments

This work was financially supported by the Korea Healthcare Technology R&D Project (A101706-1001-0000200) of MW, the Global Research Laboratory (GRL) Project, the Converging Research Program (20090081876), and the Basic Science Research Programs (20100027955 & 2012012827) of MEST.

References

[1]. American Cancer Society. Cancer Facts and Figures 2011. American Cancer Society; Atlanta, GA: 2011.

[2]. Zhao R, Li J. Perspectives on the treatment of colorectal carcinoma. World J Gastrointest Oncol. 2010; 2:229–34.

[3]. Vogelstein B, Fearon ER, Hamilton SR, Kern SE, Preisinger AC, Leppert M, et al. Genetic alterations during colorectal-tumor development. N Engl J Med. 1988; 319:525–32. [PubMed: 2841597]

[4]. Winawer SJ, Zauber AG, Ho MN, O'Brien MJ, Gottlieb LS, Sternberg SS, et al. Prevention of colorectal cancer by colonoscopic polypectomy. The National Polyp Study Workgroup. N Engl J Med. 1993; 329:1977–81. [PubMed: 8247072]

[5]. National Institutues of Cancer. Cancer Advances in Focus: Colorectal Cancer. National Institutues of Cancer; Bethesda, MD: 2010.

[6]. Kronborg O, Fenger C, Olsen J, Jorgensen OD, Sondergaard O. Randomised study of screening for colorectal cancer with faecal-occult-blood test. Lancet. 1996; 348:1467–71. [PubMed: 8942774]

[7]. Atkin WS, Edwards R, Kralj-Hans I, Wooldrage K, Hart AR, Northover JM, et al. Once-only flexible sigmoidoscopy screening in prevention of colorectal cancer: a multicentre randomised controlled trial. Lancet. 2010; 375:1624–33. [PubMed: 20430429]

[8]. Schoenfeld P, Cash B, Flood A, Dobhan R, Eastone J, Coyle W, et al. Colonoscopic screening of average-risk women for colorectal neoplasia. N Engl J Med. 2005; 352:2061–8. [PubMed: 15901859]

[9]. Pickhardt PJ, Choi JR, Hwang I, Butler JA, Puckett ML, Hildebrandt HA, et al. Computed tomographic virtual colonoscopy to screen for colorectal neoplasia in asymptomatic adults. N Engl J Med. 2003; 349:2191–200. [PubMed: 14657426]

[10]. Rex DK, Cutler CS, Lemmel GT, Rahmani EY, Clark DW, Helper DJ, et al. Colonoscopic miss rates of adenomas determined by back-to-back colonoscopies. Gastroenterology. 1997; 112:24–8. [PubMed: 8978338]

[11]. Rembacken BJ, Fujii T, Cairns A, Dixon MF, Yoshida S, Chalmers DM, et al. Flat and depressed colonic neoplasms: a prospective study of 1000 colonoscopies in the UK. Lancet. 2000; 355:1211–4. [PubMed: 10770302]

[12]. Hegde SR, Sun W, Lynch JP. Systemic and targeted therapy for advanced colon cancer. Expert Rev Gastroenterol Hepatol. 2008; 2:135–49. [PubMed: 19072376]

[13]. Petrelli N, Douglass HO Jr. Herrera L, Russell D, Stablein DM, Bruckner HW, et al. The modulation of fluorouracil with leucovorin in metastatic colorectal carcinoma: a prospective randomized phase III trial. Gastrointestinal Tumor Study Group. J Clin Oncol. 1989; 7:1419–26. [PubMed: 2674331]

[14]. de Gramont A, Figer A, Seymour M, Homerin M, Hmissi A, Cassidy J, et al. Leucovorin and fluorouracil with or without oxaliplatin as first-line treatment in advanced colorectal cancer. J Clin Oncol. 2000; 18:2938–47. [PubMed: 10944126]

[15]. Douillard JY, Cunningham D, Roth AD, Navarro M, James RD, Karasek P, et al. Irinotecan combined with fluorouracil compared with fluorouracil alone as first-line treatment for metastatic colorectal cancer: a multicentre randomised trial. Lancet. 2000; 355:1041–7. [PubMed: 10744089]

[16]. Saltz LB, Cox JV, Blanke C, Rosen LS, Fehrenbacher L, Moore MJ, et al. Irinotecan plus fluorouracil and leucovorin for metastatic colorectal cancer. Irinotecan Study Group. N Engl J Med. 2000; 343:905–14. [PubMed: 11006366]

[17]. Choi KY, Liu G, Lee S, Chen X. Theranostic nanoplatforms for simultaneous cancer imaging and therapy: current approaches and future perspectives. Nanoscale. 2012; 4:330–42. [PubMed: 22134683]

[18]. Choi KY, Min KH, Yoon HY, Kim K, Park JH, Kwon IC, et al. PEGylation of hyaluronic acid nanoparticles improves tumor targetability in vivo. Biomaterials. 2011; 32:1880–9. [PubMed: 21159377]

[19]. Choi KY, Yoon HY, Kim JH, Bae SM, Park RW, Kang YM, et al. Smart nanocarrier based on PEGylated hyaluronic acid for cancer therapy. ACS Nano. 2011; 5:8591–9. [PubMed: 21967065]

[20]. Matsumura Y, Maeda H. A new concept for macromolecular therapeutics in cancer chemotherapy: mechanism of tumoritropic accumulation of proteins and the antitumor agent smancs. Cancer Res. 1986; 46:6387–92. [PubMed: 2946403]

[21]. Hobbs SK, Monsky WL, Yuan F, Roberts WG, Griffith L, Torchilin VP, et al. Regulation of transport pathways in tumor vessels: role of tumor type and microenvironment. Proc Natl Acad Sci U S A. 1998; 95:4607–12. [PubMed: 9539785]

[22]. Maeda H. Tumor-selective delivery of macromolecular drugs via the EPR effect: background and future prospects. Bioconjug Chem. 2010; 21:797–802. [PubMed: 20397686]

[23]. Maeda H, Matsumura Y. EPR effect based drug design and clinical outlook for enhanced cancer chemotherapy. Adv Drug Deliv Rev. 2011; 63:129–30. [PubMed: 20457195]

[24]. Toole BP. Hyaluronan: from extracellular glue to pericellular cue. Nat Rev Cancer. 2004; 4:528–39. [PubMed: 15229478]

[25]. Gotte M, Yip GW. Heparanase, hyaluronan, and CD44 in cancers: a breast carcinoma perspective. Cancer Res. 2006; 66:10233–7. [PubMed: 17079438]

[26]. Choi KY, Min KH, Na JH, Choi K, Kim K, Park JH, et al. Self-assembled hyaluronic acid nanoparticles as a potential drug carrier for cancer therapy: synthesis, characterization, and in vivo biodistribution. J Mater Chem. 2009; 19:4102–7.

[27]. Choi KY, Chung H, Min KH, Yoon HY, Kim K, Park JH, et al. Self-assembled hyaluronic acid nanoparticles for active tumor targeting. Biomaterials. 2010; 31:106–14. [PubMed: 19783037]

[28]. Liu G, Choi KY, Bhirde A, Swierczewska M, Yin J, Lee SW, et al. Sticky Nanoparticles: A Platform for siRNA Delivery by a Bis(zinc(II) dipicolylamine)-Functionalized, Self-Assembled Nanoconjugate. Angew Chem Int Ed Engl. 2011

[29]. Choi KY, Saravanakumar G, Park JH, Park K. Hyaluronic acid-based nanocarriers for intracellular targeting: Interfacial interactions with proteins in cancer. Colloids Surf B Biointerfaces. 2011

[30]. Nambiar PR, Girnun G, Lillo NA, Guda K, Whiteley HE, Rosenberg DW. Preliminary analysis of azoxymethane induced colon tumors in inbred mice commonly used as transgenic/knockout progenitors. Int J Oncol. 2003; 22:145–50. [PubMed: 12469197]

[31]. Yoon SM, Myung SJ, Ye BD, Kim IW, Lee NG, Ryu YM, et al. Near-infrared fluorescence imaging using a protease-specific probe for the detection of colon tumors. Gut Liver. 2010; 4:488–97. [PubMed: 21253297]

[32]. Weber SM, Peterson KA, Durkee B, Qi C, Longino M, Warner T, et al. Imaging of murine liver tumor using microCT with a hepatocyte-selective contrast agent: accuracy is dependent on adequate contrast enhancement. J Surg Res. 2004; 119:41–5. [PubMed: 15126080]

[33]. Boivin GP, Washington K, Yang K, Ward JM, Pretlow TP, Russell R, et al. Pathology of mouse models of intestinal cancer: consensus report and recommendations. Gastroenterology. 2003; 124:762–77. [PubMed: 12612914]

[34]. Mitchell BS, Whitehouse A, Prehm P, Delpech B, Schumacher U. CD44 exon variant 6 epitope and hyaluronate synthase are expressed on HT29 human colorectal carcinoma cells in a SCID mouse model of metastasis formation. Clin Exp Metastasis. 1996; 14:107–14. [PubMed: 8605724]

[35]. Richter U, Wicklein D, Geleff S, Schumacher U. The interaction between CD44 on tumour cells and hyaluronan under physiologic flow conditions: implications for metastasis formation. Histochem Cell Biol. 2012; 137:687–95. [PubMed: 22270319]

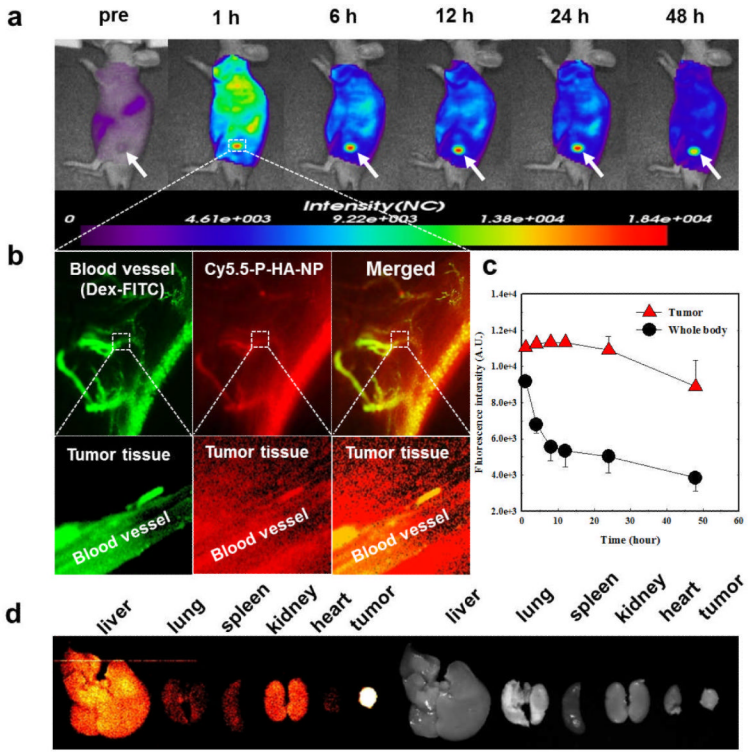

Figure 1. NIRF imaging of small-sized HT29 colon tumors

(a) Whole body images of athymic nude mice bearing HT29 tumors after intravenous injection of Cy5.5-P-HA-NPs as a function of time. Arrows indicate the sites of tumors. (b) Intravital fluorescence images of tumor vasculature and Cy5.5-P-HA-NPs. (c) Quantification of the NIRF intensities in the whole bodies and tumor tissues were estimated from the mean fluorescence intensities in 1000 mm^2 for whole bodies and in 25 mm^2 for the tumor tissues. Error bars represent the standard deviation (n=3). (d) *Ex vivo* fluorescence images of organs and tumor excised at 48 h post-injection of NPs (5mg/kg).

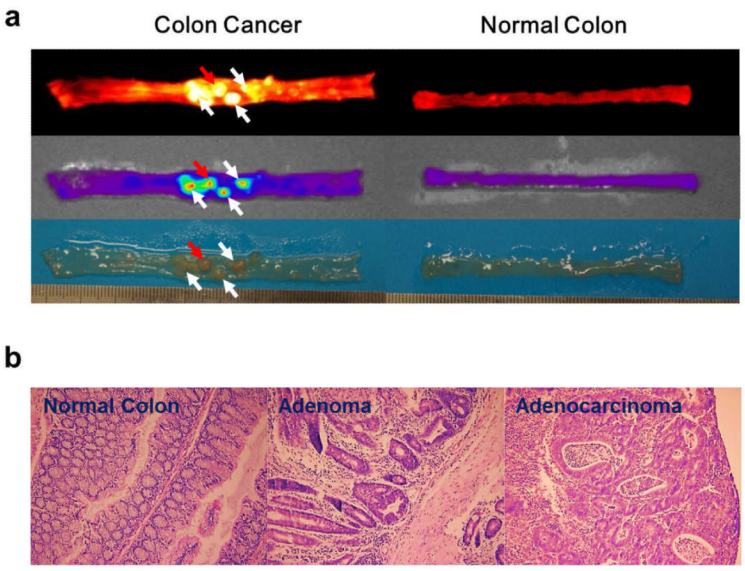

Figure 2. NIRF imaging of early-stage orthotopic colon tumors

(a) Representative colon images of AOM-induced orthotopic colon cancer models after intravenous injection of Cy5.5-P-HA-NPs. White and red arrows indicate adenomas and adenocarcinomas, respectively. (b) Representative histological images of normal colon, adenoma and adenocarcinoma slices stained using hematoxylin and eosin.

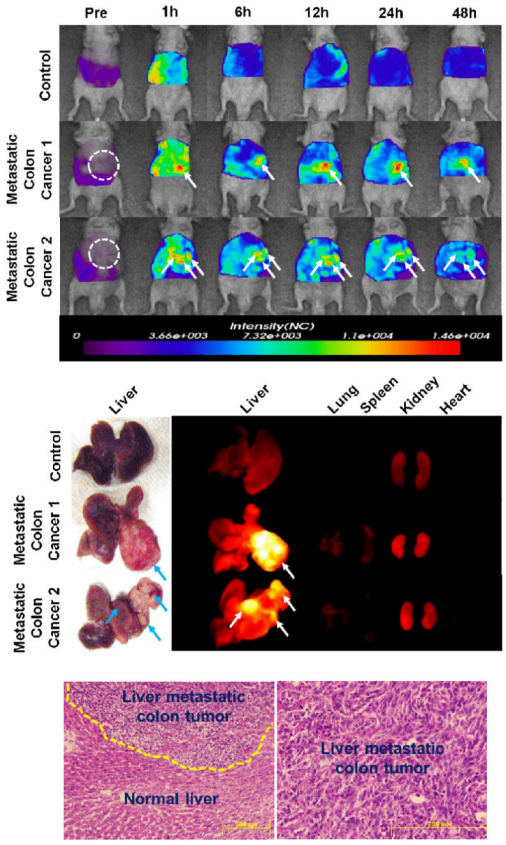

Figure 3. NIRF imaging of liver-implanted CT26 colon tumors

(a) Whole body images of athymic nude mice bearing CT26 colon tumors in their liver tissues after intravenous injection of Cy5.5-P-HA-NPs as a function of time. Arrows indicate the sites of tumors. (b) *Ex vivo* fluorescence images of tumor-bearing livers and organs excised at 48 h post-injection of NPs (5mg/kg). (c) Representative histological images of normal liver and tumor slices stained with hematoxylin and eosin.

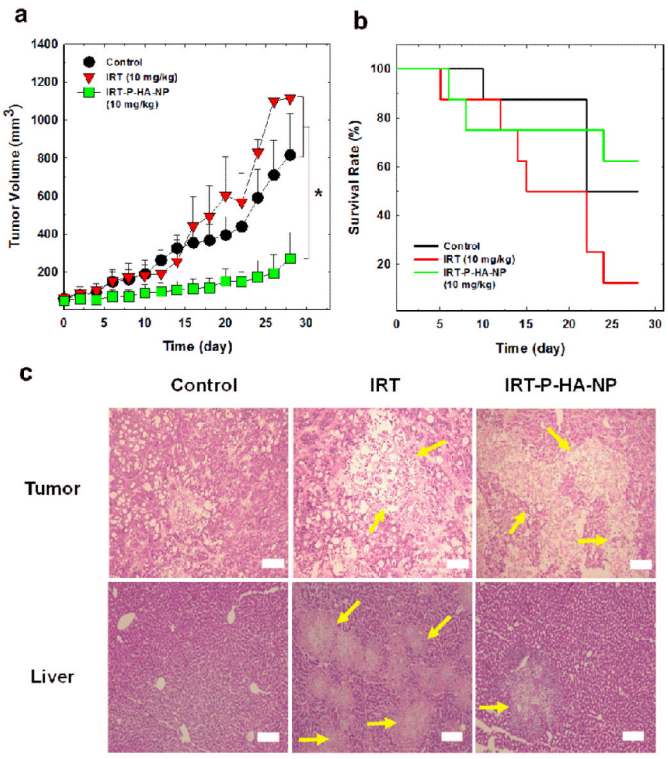

Figure 4. Therapeutic efficacy of IRT-P-HA-NPs

(a) Tumor growth and (b) survival rate of HT29 human colon cancer xenografts treated with saline, free IRT and IRT-P-HA-NPs at a dose of 10 mg IRT/kg. (c) Representative histological images of liver and tumor slices stained using hematoxylin and eosin. The organs were excised at 30 days after the start of administration. Arrows indicate necrosis in tissues. Asterisk symbols (*) denote statistically significant differences (*: $p<0.05$) calculated using the one-way ANOVA test. Error bars in a and b represent standard deviations (n=8).

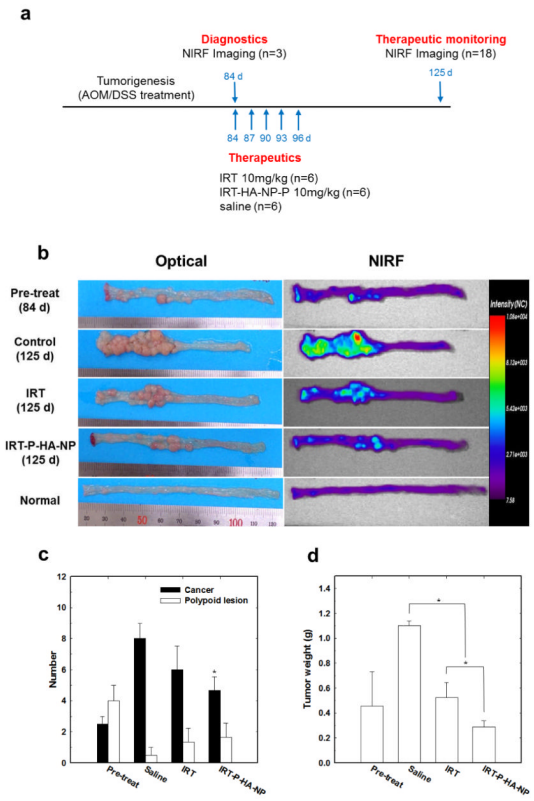

Figure 5. Therapeutic monitoring of orthotopic colon tumors

(a) Diagram of the general procedure (b) Representative colon images of AOM/DSS-induced orthotopic colon cancer models that were pre-treated or treated with saline, IRT or IRT-P-HA-NPs. Images acquired at 6 h after intravenous injection of Cy5.5-P-HA-NPs. White and red arrows indicate adenomas and adenocarcinomas, respectively. Quantitative results of (c) histological polyp examination and (d) tumor weight. Asterisk symbols (*) denote the statistically significant differences (*: $p<0.05$) calculated using the one-way ANOVA test. Error bars in a and b represent the standard deviations (n=6).

Table 1

Characteristics of IRT-Loaded P-HA-NPs

Samples	Loading Contents (%)	Loading Efficiency (%)	Mean Diameter (nm)
P-HA-NP	--	--	255.7 ± 2.9
IRT 10%-P-HA-NP	9.69 ± 0.1	96.97 ± 0.9	144.8 ± 1.5
IRT 20%-P-HA-NP	13.23 ± 0.1	66.16 ± 0.7	168.8 ± 10.7
IRT 30%-P-HA-NP	18.74 ± 0.5	62.49 ± 1.5	238.3 ± 6.9
IRT 40%-P-HA-NP	18.85 ± 0.3	47.13 ± 0.7	287.0 ± 4.0
IRT 50%-P-HA-NP	21.05 ± 0.8	42.1 ± 1.7	404.0 ± 14.5